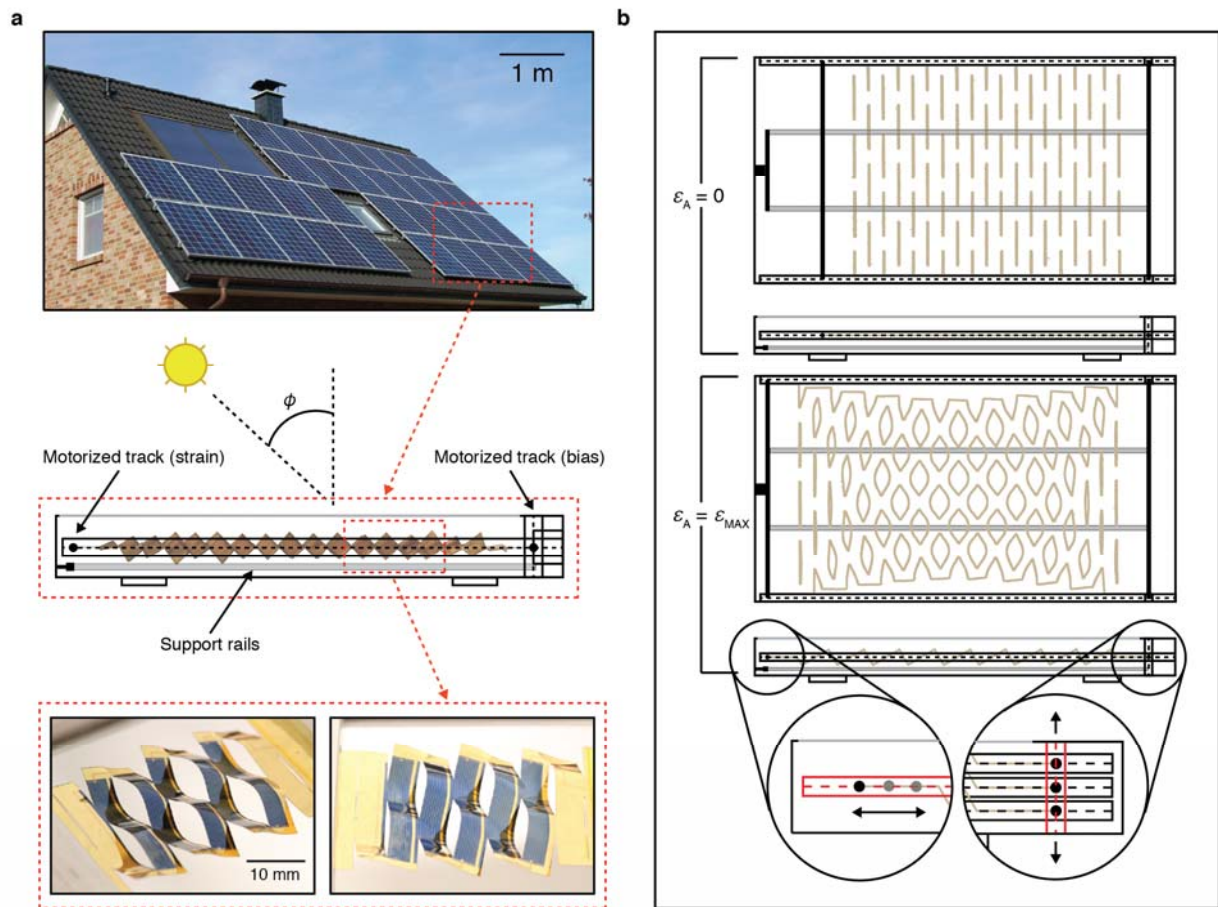**Supplementary Figure 1**

Rooftop kirigami tracking and schematics of module. (a) Thin-film kirigami constructs may be integrated with low-profile, rigid enclosures to ensure weatherproofing and compatibility with existing rooftop installation hardware. Tensioned support cables may be used in large arrays support system weight and prevent sagging of the structure. **(b)** Schematic view of kirigami tracking system when $\varepsilon_A = 0$ and also maximum strain (i.e. $\varepsilon_A = \varepsilon_{MAX}$). Note the detailed views of each motorized track, which are used to provide strain and vertical biasing during operation.
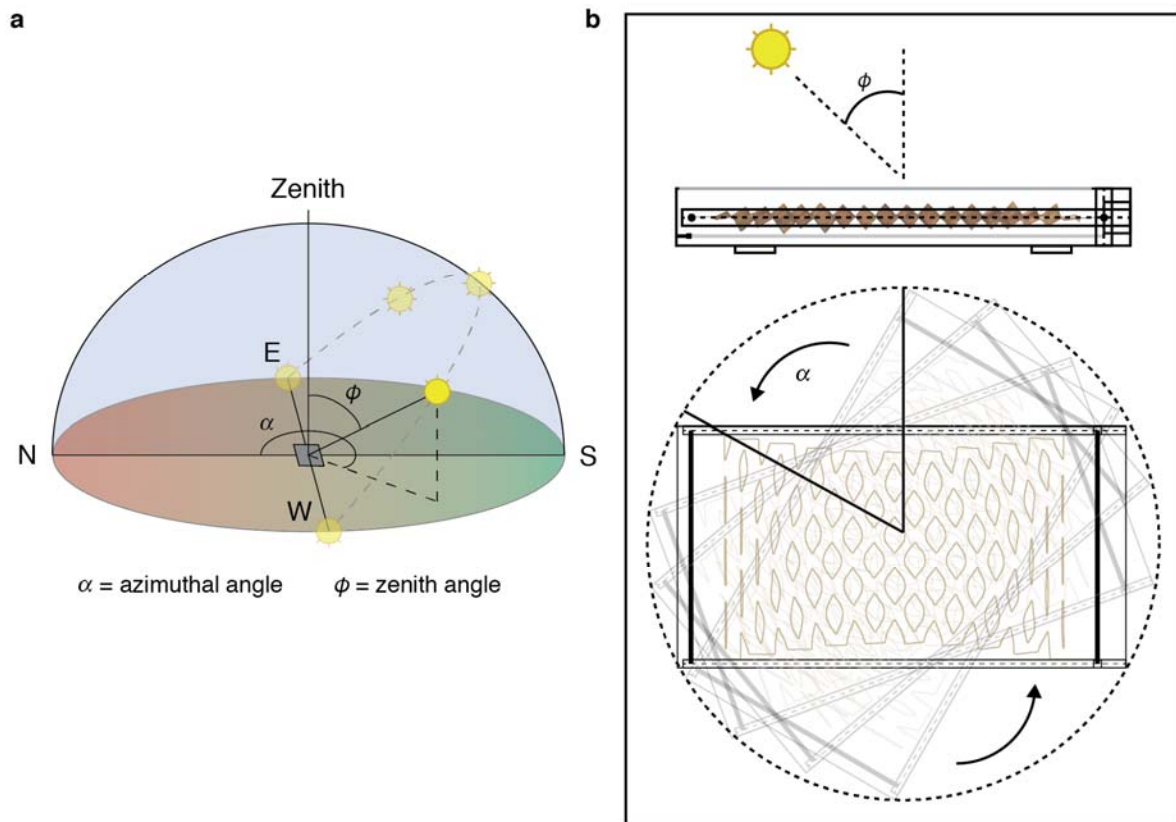
Dual-axis tracking using kirigami tracker. **(a)** The azimuthal (α) and zenith (ϕ) angles fully characterize the trajectory of the sun as a function of time of day, time of year, and geographic location. **(b)** To enable dual-axis tracking, the proposed kirigami tracker need simply be rotated about its base to track the azimuth of the sun.

Supplementary Figure 3
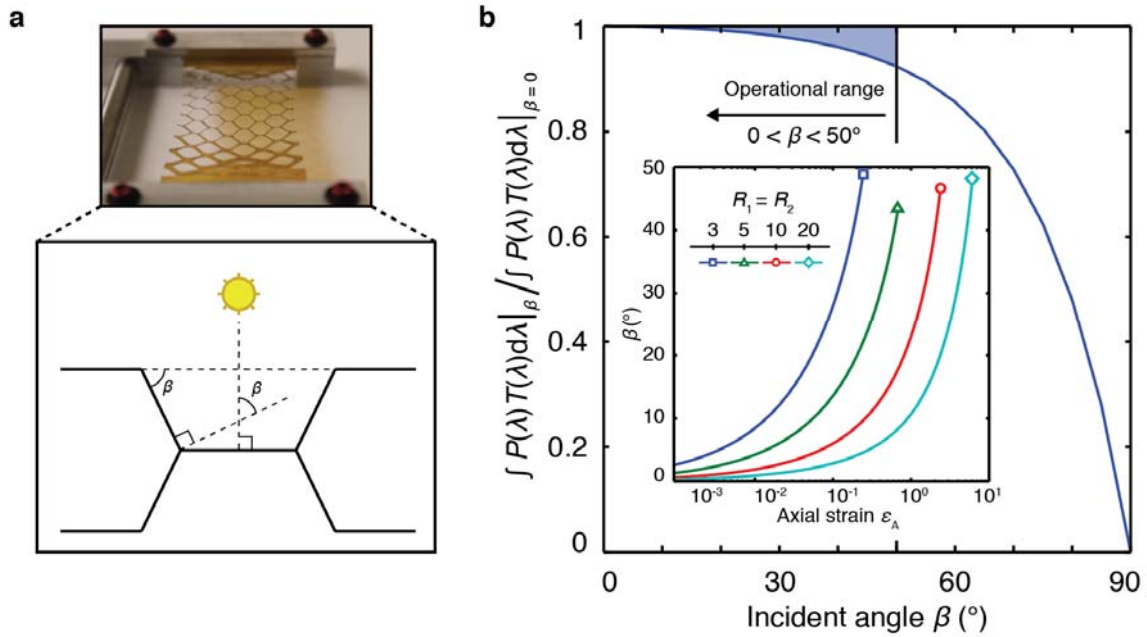
Surface reflection losses and anti-reflection coating. **(a)** Due to the bowing of the kirigami tracker out of the original plane of the sheet, we must account for oblique angle incidence and any reflection losses as a function of angle, β. **(b)** Normalized transmitted power integrated from 350 to 900 nm *vs.* β for the bilayer ARC (49 nm TiO_2 and 81 nm MgF_2) used in this study. Incident power, $P(\lambda)$, was taken as AM1.5G, and transmission, $T(\lambda)$, was calculated using common transfer matrix methods. *Inset:* β *vs.* axial strain, ε_A, for $R_1 = R_2 = 3, 5, 10,$ and 20. Interestingly enough, while each sample tracks to a different maximum ε_A (according to the principles of optimal tracking outlined in Fig. 3), β at ε_A (max) remains consistent, and below 50°. Thus, we conclude $0° < \beta < 50°$ signifies the operating range for tracking, over which normalized transmission is shown to remain relatively constant.
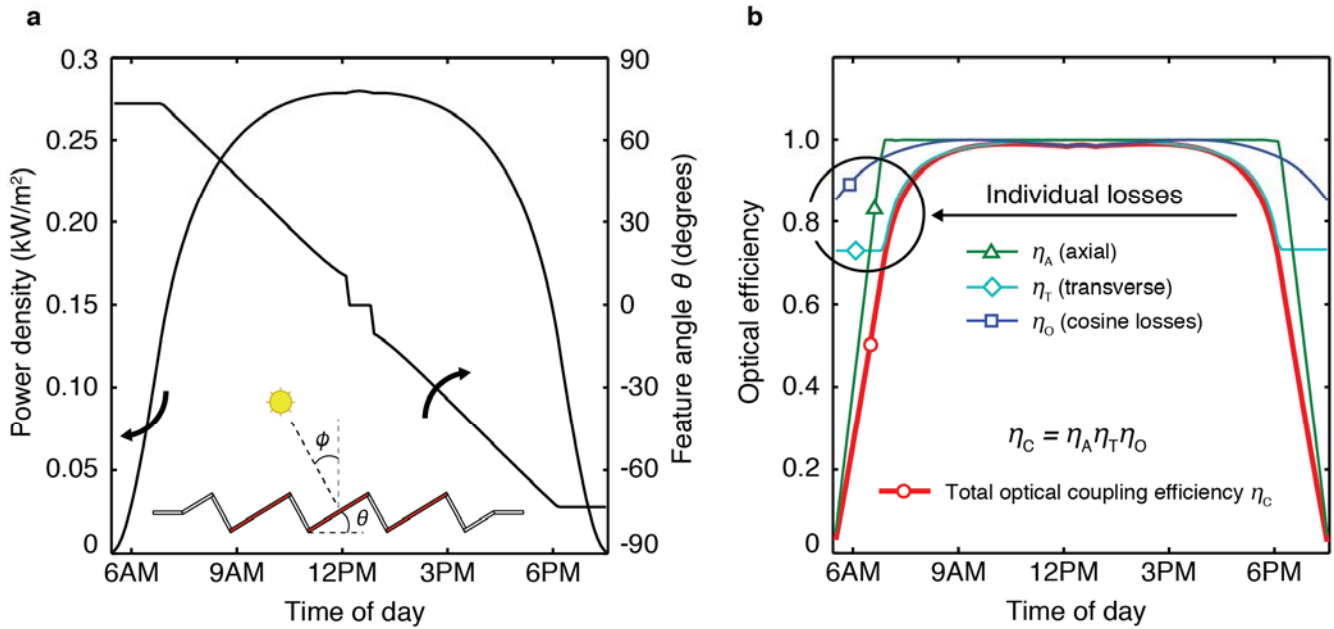
Additional system response and optical efficiency breakdown. **(a)** Power density and feature angle, θ, *vs.* time of day for a kirigami tracking structure in Phoenix, AZ (33.45° N, 112.07° W) during the summer solstice, where $R_1 = R_2 = 5$. PCE was assumed to be 20%. **(b)** Individual optical loss mechanisms for a kirigami tracking structure in Phoenix, AZ during the summer solstice, where $R_1 = R_2 = 5$. The total optical efficiency is also shown.
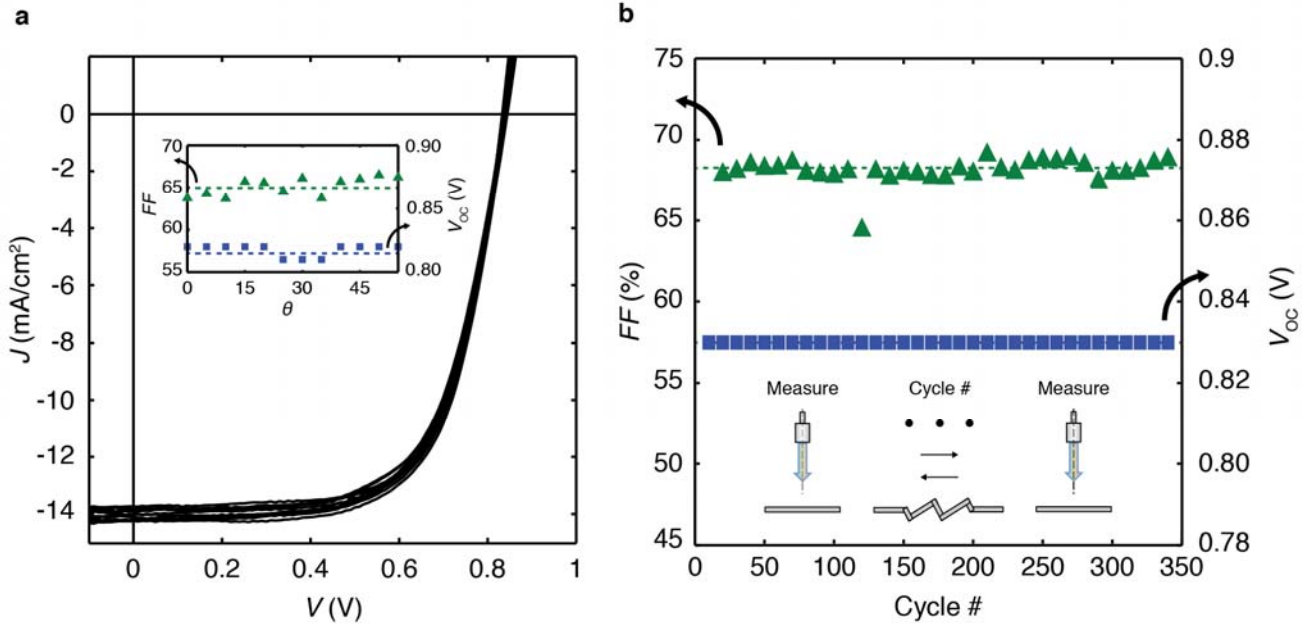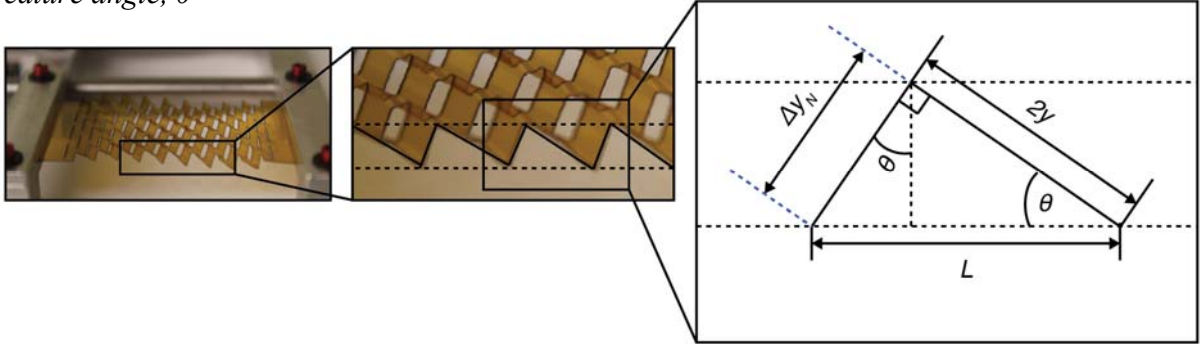
Effect of cycling on electrical response for kirigami tracker. **(a)** J-V characteristics for a Kapton®/GaAs tracker where $R_1 = R_2 = 5$ at incremental angles of simulated AM1.5G incidence at 1 sun (100 mW/cm^2) intensity, oriented normal to the surface of the solar cells (i.e. $\phi = \theta$). Inset: Fill factor, FF, and open circuit voltage, V_{OC}, show no appreciable degradation up until the optimal θ^*, and the variation as shown (±1.1 and ±4.5 mV for FF and V_{OC}, respectively) is attributed to the error in control over feature angle ($\pm1.0°$, as noted earlier in the text). The power conversion efficiency of these devices under 1 sun AM1.5G illumination was $7.4 \pm 0.1\%$ at the outset, with virtually no degradation upon cycling. **(b)** FF and V_{OC} *vs.* cycle number for a Kapton®/GaAs tracker, where $R_1 = R_2 = 5$. There was no systematic change in FF or V_{OC}, with the random variation in measurements due to error in control over feature angle.

Supplementary Note 1
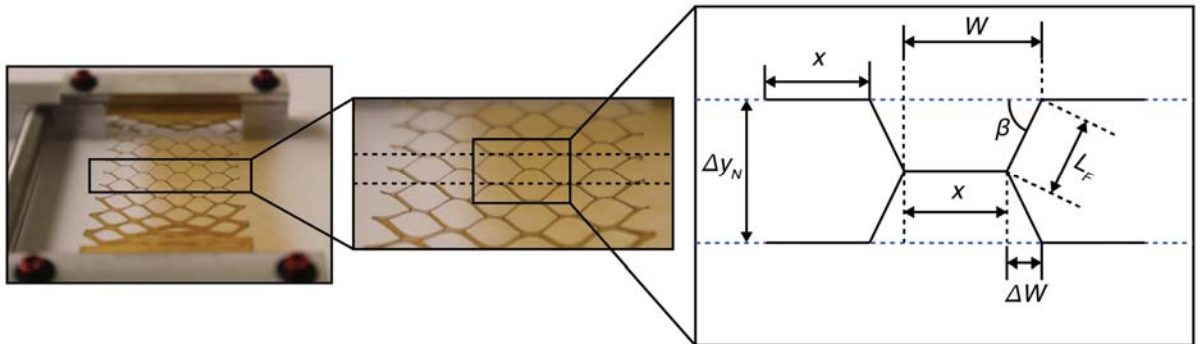
Derivation of geometric response

Feature angle, θ

$$L_0 = 2y \tag{1}$$

$$L = \frac{2y}{\cos\theta} \tag{2}$$

$$\Delta y_N = 2y\tan\theta \tag{3}$$

$$\varepsilon_A = \frac{L - L_0}{L_0} = \frac{1}{\cos\theta} - 1 \quad \rightarrow \quad \theta = \cos^{-1}\left(\frac{1}{\varepsilon_A + 1}\right) \tag{4}$$

Transverse strain, ε_T

$$W_0 = x + L_F \tag{5}$$

$$W = x + \Delta W \tag{6}$$

$$\varepsilon_T = \frac{W - W_0}{W_0} = \frac{L_F\cos\beta - L_F}{x + L_F} \tag{7}$$

where:

$$\Delta W = L_F \cos \beta \tag{8}$$

$$\beta = \sin^{-1}\left(\frac{y \tan \theta}{L_F}\right) \tag{9}$$

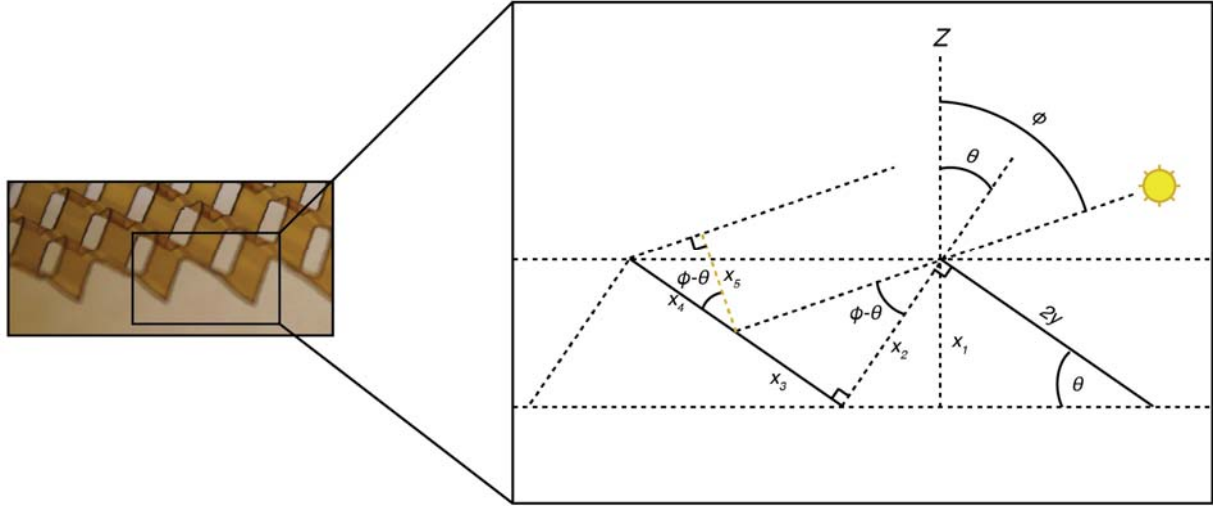$$L_F = \frac{L_C - x}{2} \tag{10}$$

Substituting ΔW, β, and L_F and using $R_1 = L_C / x$ and $R_2 = L_C / y$ to non-dimensionalize, simplification of ε_T yields:

$$\varepsilon_T = \frac{R_1 - 1}{R_1 + 1}\left[\cos\left(\sin^{-1}\left(\frac{2R_1 \tan \theta}{R_1 R_2 - R_2}\right)\right) - 1\right] \tag{11}$$

7

Supplementary Note 2

Derivation of coupling efficiency, η_C

To determine the total coupling efficiency, η_C, we must account for individual optical coupling efficiencies in the axial (η_A) and transverse (η_T) directions, as well as cosine losses (η_O) and surface reflection (η_R) at oblique incident angles:

$$\eta_C = \eta_A \eta_T \eta_O \left(1 - \eta_R\right) \tag{12}$$

In the presence of a suitable anti-reflective coating (ARC) (such as the TiO_2/MgF_2 bilayer ARC used in this paper, see Supplementary Fig. 3), η_R becomes negligible such that:

$$\eta_C = \eta_A \eta_T \eta_O \tag{13}$$

Using the supplemental figure above to determine η_A:

$$x_1 = 2y\sin\theta \tag{14}$$

$$x_2 = \frac{x_1}{\cos\theta} = 2y\tan\theta \tag{15}$$

$$x_3 = x_2 \tan(\phi - \theta) = 2y\tan\theta\tan(\phi - \theta) \tag{16}$$

$$x_4 = 2y - x_3 = 2y - 2y\tan\theta\tan(\phi - \theta) = 2y\left[1 - \tan\theta\tan(\phi - \theta)\right] \tag{17}$$

$$\eta_A = \frac{x_4}{2y} = 1 - \tan\theta\tan(\phi - \theta) \text{ for } \phi > \theta \tag{18}$$

else $\eta_A = 1$ (19)

$$\eta_T = \frac{W}{W_0} = \varepsilon_A + 1 \tag{20}$$

$$\eta_O = \cos\gamma \tag{21}$$

where γ is the angle between the normal to the cell and the source:

$$\gamma = \cos^{-1}\left(\frac{a \cdot b}{|a||b|}\right) \tag{22}$$

where:

$$a = \begin{bmatrix} -\sin\phi\cos\alpha & \sin\phi\sin\alpha & \cos\phi \end{bmatrix} \tag{23}$$

and (for a panel with an E-W axis of rotation as was used in Phoenix, AZ during this study):

$$b = \begin{bmatrix} 0 & -\tan\theta & -1 \end{bmatrix} \tag{24}$$

Here, ϕ is the zenith angle, α is the azimuthal angle as measured clockwise from North, and θ the feature angle of the kirigami tracking structure.

Thus, for a kirigami tracking system with an E-W axis of rotation:

$$\eta_C = \eta_A\eta_T\eta_O = \left[1 - \tan\theta\tan(\phi - \theta)\right]_0^1 (\varepsilon_A + 1)\cos\gamma \tag{25}$$

For the case when the optical source is moving in the plane normal to the tracking axis (as per the figure above), cosine losses are solely dependent on θ and ϕ:

$$\eta_O = \cos(\phi - \theta) \tag{26}$$

$$\eta_C = \eta_A\eta_T\eta_O = \left[1 - \tan\theta\tan(\phi - \theta)\right](\varepsilon_A + 1)\cos(\phi - \theta) = (\varepsilon_A + 1)\sec\theta\cos\phi \tag{27}$$

where:

$$\theta = \cos^{-1}\left(\frac{1}{\varepsilon_A + 1}\right) \tag{4}$$

Upon simplifying, η_C may be written as:

$$\eta_C = \cos\phi\left(\varepsilon_A + 1\right)\left(\varepsilon_T + 1\right) \tag{28}$$